Acoustically Driven Sorption Heat Pump

Ariel Vardi-Chouchana◉† and Guy Z. Ramon◉*

¹*The Nancy and Stephen Grand Technion Energy Program, Department of Civil & Environmental Engineering, Technion – Israel Institute of Technology, Haifa 32000, Israel*

Recent years have seen a dramatic rise in global cooling demand, driven by economic growth and climate change, and resulting in an increasing share of the total electric power consumption. Meanwhile, the ubiquitous vapor-compression air conditioners use refrigerants, which contribute greatly to global emission of greenhouse gases. In order to reduce the strain on electric grids, heat-driven technologies must be developed. Here, an acoustic driven sorption cooling device is examined experimentally and theoretically. The device can potentially utilize heat or electricity as a power input, uses environmentally benign working fluids, and offers simple, reliable construction with little to no moving parts. The results demonstrate the sorption-mediated, time-averaged heat-transfer mechanism, driven by the acoustic field. An unoptimized, proof-of-concept device is operated using a mixture of atmospheric air and either water or methanol, with cordierite and zeolite sorbents. The device is able to achieve temperature differentials $> 30\,^\circ$C. Moreover, a coefficient of performance of approximately 3 (based on the acoustic power input) is achieved at a temperature difference of $10\,^\circ$C. Theoretical calculations provide an outlook on the operation of such technology, compared with existing cooling technologies, demonstrating its potential for achieving high efficiencies. Finally, prospects for further development are discussed.

I. INTRODUCTION

The demand for cooling, especially air conditioning (AC), is on the rise, tripling its share of the global energy consumption worldwide between 1960 and 2016, and projected to triple once more by 2050 [1]. This increasing demand is already a considerable strain on energy grids, and contributes 8% of global CO_2 emissions—expected to reach 15% by 2050. The trend of cooling demand growth is prevalent in hotter countries, especially those undergoing major economic growth. According to a recent report by the International Energy Agency (IEA), the number of AC units worldwide is expected to increase considerably, and already is, especially in China and India, as can be seen in Fig. 1 [1]. To accommodate this change, major improvements in the energy efficiency and environmental impact of AC units are essential [2].

Currently, space cooling is dominated by electricity-driven vapor-compression devices, which typically utilize hydrofluorocarbon-based (HFC) or other harmful materials as the working fluid, following the ban of hydrochlorofluorocarbons (HCFCs) and chlorofluorocarbon-based (CFC) refrigerants as part of the agreements reached in the Montreal protocol [3]. Recent ongoing efforts to discontinue the use of HFCs, which is also a big contributor to global-warming potential, has seen some success in developed countries, such as in around 25 states in the USA as part of the United States Climate Alliance. The progress in trying to combat climate change is encouraging, but stays limited in developing countries, such as China and India, where strong economic and social development shadows the needs of our climate. These materials, harmful to our planet's atmosphere, are released when devices using them are disposed. In fact, the think tank "Project Drawdown" recently concluded that the phasing out and better handling of these refrigerants is the best course of action for reducing the amount of CO_2 equivalents released to the atmosphere, while generating a significant capital profit [4]. As a result of this need, various cooling technologies are currently being investigated as potential replacements. Such alternative cooling technologies should provide high efficiency, use nonharmful working fluids, have good scalability, and a small form factor (see the Supplemental Material for a short summary of existing alternative technologies [5]).

Acoustically driven cooling, which utilizes acoustic mechanical power to drive a heat pump, is known

---

*ramong@technion.ac.il

†Present address: Department of Mechanical Engineering, Massachusetts Institute of Technology, Cambridge, Massachusetts 02139, USA and Applied Ocean Physics and Engineering Department, Woods Hole Oceanographic Institution, Woods Hole, Massachusetts 02543, USA.
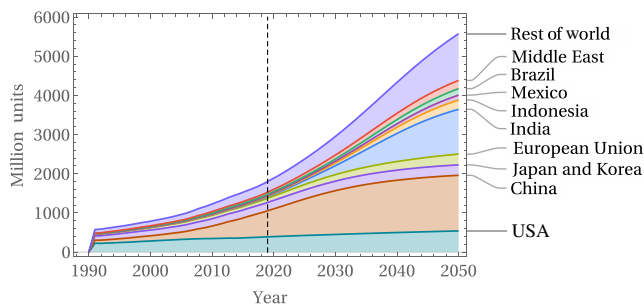
FIG. 1. Number of household AC units between 1990 and 2050, adapted from data reported by the International Energy Agency (IEA) [1].

as thermoacoustic refrigeration and has been studied extensively over the past few decades. Previous studies have shown that the theoretically achievable efficiencies, for standing-wave thermoacoustic systems, can reach 40%–50% of the Carnot efficiency [6] and 57% when using a traveling-wave device [7]. A standing-wave refrigerator was employed on the space shuttle Discovery, able to operate at 20% of the Carnot efficiency [8]. While vapor-compression devices can achieve up to 60% efficiency, they rely on refrigerants, which increase global-warming potential, and optimal mechanical compressors in order to achieve such high efficiencies. Thermoacoustic devices use environmentally benign gases, eliminating the environmental impact caused by refrigerants. Thermoacoustic devices can be driven using both thermal power—via a thermoacoustic engine that produces acoustic power from heat [9], recently shown to be achievable at very low temperatures [10,11]), or by electricity—using an acoustic driver. Electroacoustic conversion efficiencies can achieve very high values when using commercially available linear alternators [12,13]. Using heat can reduce the strain on electricity grids, with adsorption and absorption heat pumps being the more viable options in that category, as they enable use of waste heat as a power source. Absorption systems have penetrated the refrigeration market where heat is readily available and is cheaper than electricity, but still face challenges at small scale, due to cost, complexity and footprint, if continuous operation is sought [14], making them more appropriate for larger-scale implementation. Similarly, adsorption-based systems have yet to find success in heat-driven cooling applications due to improvements still needed in the characteristics of adsorbents, as well as system design and control [15].

Herein, we introduce acoustic driven sorption cooling, which can utilize heat as a power source, uses environmentally benign working fluids, has little to no moving parts and, as shown, can achieve high efficiencies, potentially competing with and even surpassing existing technologies, including vapor compression and sorption-based systems. The classical mechanism of a thermoacoustic heat pump

relies on the heat transferred between the working fluid and a solid surface, due to temperature gradients created during the acoustic cycle—compression and expansion and motion; herein, we refer to this mode as *conduction-based* thermoacoustic cooling. These systems consist mainly of an acoustic resonator filled with an inert gas, which sustains a monofrequency acoustic wave driven by an acoustic driver, such as a linear alternator or a loudspeaker. In it, a stack of plates (or another form of porous media) is located at an optimal position along which a heat flux is created using the thermoacoustic cycle. Usually, two heat exchangers are placed at both ends of the stack. A simple diagram of such a system can be seen in Fig. 2(a). To date, all such systems employed the classical thermoacoustic cycle using various designs based on these components [13,16].

In contrast, the mechanism underlying our proposed system introduces mass exchange via sorption, offering a more efficient mode of heat transfer where latent heat is transferred between the working fluid, a mixture in which at least one component may undergo sorption, and the boundary (a sorbent material). We note that, in the general context, sorption may refer to either the adsorption of a gas component onto a suitable solid surface, or the absorption into a suitable liquid solution. The process is analogous to the operation of sorption heat pumps, but instead of using temperature swings to sorb and desorb a working fluid, an acoustic wave drives a pressure-swing sorption and desorption cycle. We refer to this as *sorption-based* thermoacoustic cooling and its proposed operation can be conceptualized using a four-step process, as shown schematically in Fig. 2(b). During the cycle, the fluid undergoes both compression and expansion while moving longitudinally back and forth. During the compression stage, the partial pressure of the sorbing gas increases, driving its sorption onto the boundary. The parcel is then displaced as it undergoes expansion, which reduces the partial pressure of the sorbing gas and allows the release of the sorbing component from the boundary. The combined motion and boundary exchange results in a mass flux, generated by the acoustic field, as previously demonstrated [17,18] to be a time-averaged product of the velocity and concentration fields, here depicted by a simplified four-step cycle. In the present work, we further consider the heat flux generated along the direction of wave propagation via the transfer of latent heat that accompanies mass transfer through sorption and desorption, and its ability to efficiently function as a heat pump. A proof-of-concept device is presented in this paper, along with a mathematical model used to verify its operation and, ultimately, its projected performance.

II. EXPERIMENTAL SYSTEM

In order to establish an experimental proof of concept for the sorption-mediated heat-pumping mechanism
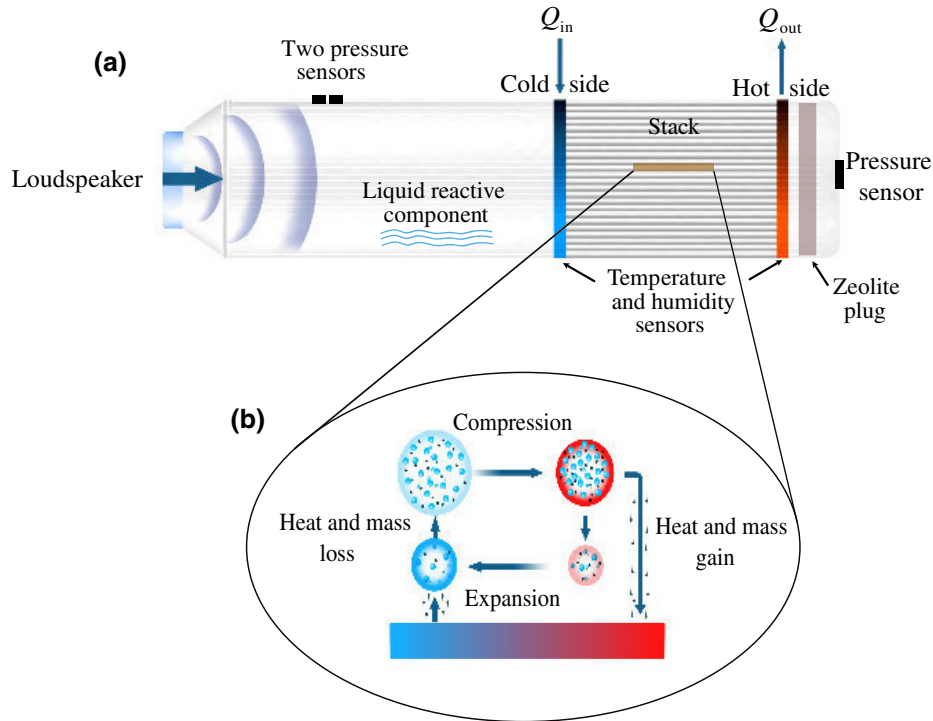
FIG. 2.   (a) Diagram of the experimental system used to demonstrate the sorption, acoustic driven cooling mechanism. (b) Schematic representation of the sorption-based mechanism that creates a net mass and heat flux along the surface of the stack.

described above, a simple acoustic heat pump is constructed and tested. The system comprises an acoustic driver connected to a closed-ended tube (resonator), in which the sorbent material is placed (see Fig. 2(a) for a schematic diagram of the system).

Specifically, the main components of the heat pump are a stainless-steel tube, 4.5 cm in diameter and 69 cm in length, attached to an 8" loudspeaker (Polk-Audio 4 Ohm subwoofer, model db840DVC). The solid sorbent used is a 10-cm-long 600 CPSI (cells per square inch, corresponding to square channels size with a spacing of 1 mm) Cordierite honeycomb acting as a "stack" of plates along which the mass and heat flux flow generated by the proposed four-step process. The system is driven at a frequency of 122 Hz, resulting in a quarter wavelength standing acoustic wave (see Sec. 2 within the Supplemental Material for the acoustic characterization of the system [5]). The stack is located 5.5 cm from the resonator's closed end, corresponding to 0.15 of the quarter wavelength, a generally favorable position for the operation of a thermoacoustic heat pump [19]. Thermocouples are located at both ends of the stack to measure the temperature difference generated along the stack due to heat pumping. Water humidity sensors are located outside of the stack, at both ends, allowing measurement of the concentration of water vapor (during experiments where water

was used as the primary sorbing species in the gas mixture). A pressure transducer is located at the closed end of the resonator to measure the absolute mean pressure in the resonator and the pressure amplitude of the acoustic wave. Two differential pressure transducers are located near the loudspeaker, spaced at 2.4 cm apart, to measure the acoustic power, $\dot{E}$, supplied to the resonator by the loudspeaker [20]. We note that the presence of the stack located inside the loudspeaker does not significantly disrupt the acoustic field (see Fig. S8 within the Supplemental Material [5]). A heat load is delivered to the system by Nichrome wires wrapped over the edge of the cold side of the honeycomb stack. This, along with the acoustic power measurements, enabled determination of the heat-pump performance in terms of its coefficient of performance (COP) (see Sec. 2 within the Supplemental Material for more information on the experimental system [5]).

In order to generate the desired mass flux along the stack, a concentration gradient of the sorbing species is necessary. To achieve that, a piece of paper soaked with the sorbing component (in liquid phase) is placed near the cold side of the stack. This enforces the vapor pressure to be close to saturation at the temperature of the cold side, corresponding with the maximum available vapor concentration. At the hot side, a low vapor concentration is required, and this is enforced by a mesh plug, filled with

zeolite 13X pellets, which is inserted into the resonator channel [see schematic illustration in Fig. 2(a)].

We note that our current setup operates in a batch mode, which is particularly limited by the hot-side sorbent tasked with removing material from the system. Introducing and removing material from the resonator is required by employing continuous "mass exchangers," and poses a future engineering challenge. Potential solutions appear to already exist and we discuss these in the conclusions section. Nevertheless, the batch operation employed herein provides a proof of concept of the proposed method.

The zeolite plug keeps the hot side at a low concentration as long as it maintains some adsorption capacity. Both the liquid and zeolite plug are not in direct contact with the stack and so transport of the sorbing component from one side to the other is primarily due to mass streaming [17]. The main possible bottleneck arising in such a configuration is diffusion of the sorbing component from the liquid pool to the cold side of the stack and from the hot side of the stack to the zeolite plug. Therefore, the distance between the mass source or sink and the stack is set at around one acoustic displacement [9].

The main gas mixture used in our experiments is comprised of air as the *inert* component and water as the *sorbing* component. Methanol and ethanol are also used, so as to assess the device's performance with more volatile liquids, corresponding with higher concentrations of the sorbing species in the mixture; however, no concentration measurements are made with these mixtures. In a separate set of experiments, measurements are made of the temperature difference across the stack, generated at a given COP set by the acoustic power delivered to the system and the heat load imposed on the stack. In these, only the air-water mixture is used so that concentration measurements could also be made, crucial for a clear understanding of the stages of the experiment.

III. MODEL FORMULATION

To model the transport processes occurring in the system, we consider a cylindrical tube of length L and diameter d where $d \ll L$, which acts as the resonator. A section of the resonator tube is filled with a porous material (referred to hereafter as the *stack*) comprised of closely packed parallel channels, each with a hydraulic radius $h \ll d$ and length L_s. The resonator contains a gas mixture with an *inert* component and a *sorbing* component, which is able to sorb and desorb onto the solid surface of the stack's channel walls; we denote each component with the subscripts i and r, respectively (see Fig. 3 for a schematic representation of the model geometry).

In what follows, we consider all model variables as a sum of a time harmonic, oscillating part and a time-averaged, mean part, via

$$\xi = \xi_m(x) + \xi_1(x,y)e^{i\omega t}, \tag{1}$$

where ξ denotes any oscillating parameter in the system, with subscripts m and 1 denoting the mean and oscillating part, respectively. Here, ω is the angular frequency of oscillation, t is the time, and x, y denote the longitudinal and transverse coordinates, respectively.

A. Reversible sorption under oscillating pressure

The main feature of the system under consideration is the reversible heterogeneous reaction (sorption and desorption of the reactive component) occurring at the boundary, driven by the pressure oscillations of the acoustic field. Following Weltsch *et al.* [17], we may write the conservation of species equation for the reactive component as

$$i\omega C_1 + u_1 \frac{\partial C_m}{\partial x} = D \frac{\partial^2 C_1}{\partial y^2}, \tag{2}$$

in which C is the concentration, in terms of the molar fraction of the reactive component within the mixture, u_1 is the oscillating axial velocity, and D is the diffusion coefficient. To solve this second-order ordinary differential equation (ODE) for C_1 in y, two boundary conditions are needed. The first boundary condition is simply symmetry at the midplane, $y = 0$,

$$\frac{\partial C_1}{\partial y} = 0, \quad y = 0. \tag{3}$$

The second boundary condition is derived from the reversible reaction at the channel wall, $y = h$, which we write as

$$\dot{N}_r = B_s \frac{d\theta}{dt} = i\omega B_s \theta_1 e^{i\omega t}, \quad y = h, \tag{4}$$

where θ, an oscillating parameter, is the fraction of the sorbent capacity, B_s, which is occupied by the sorbed species. $\dot{N}_r$ is the first-order molar flux of the reactive component at the boundary, composed of diffusive and convective terms,

$$\dot{N}_r = C\dot{N} + N_m D \frac{\partial C}{\partial y}, \tag{5}$$

with $\dot{N}$ the total molar flux at the boundary and N as the total molar concentration of the gas mixture. Since no sorption of the inert species occurs at the boundary, it follows that $\dot{N} = \dot{N}_r + \dot{N}_i = \dot{N}_r$ (where $\dot{N}_i$ is the molar flux of the
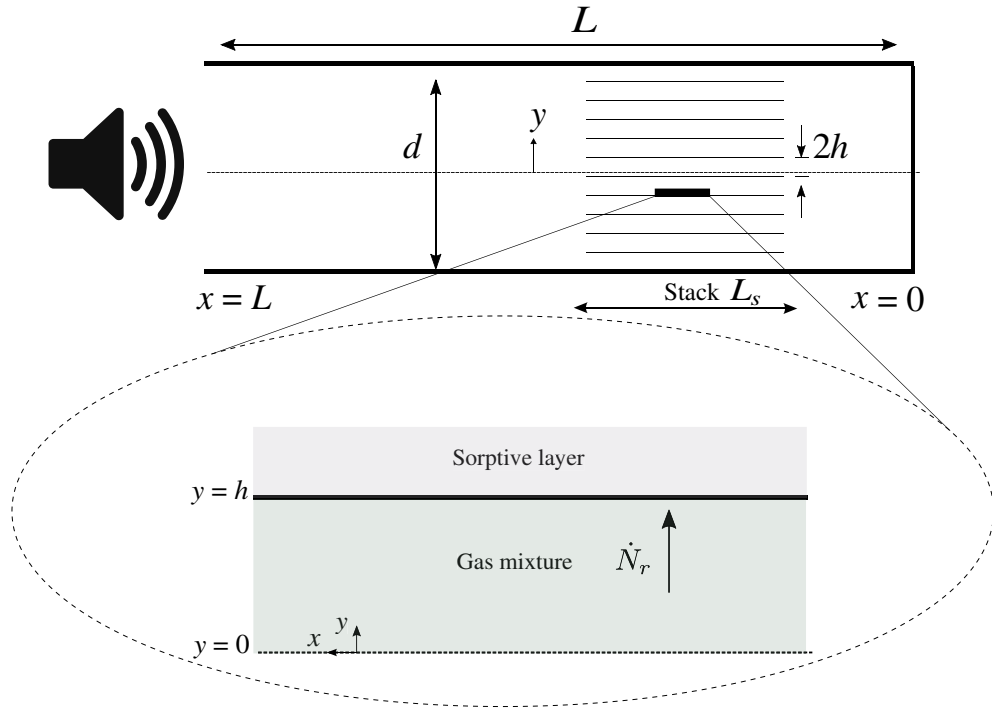
FIG. 3.   Schematic drawing of the modeled configuration.

inert species), so that

$$\dot{N}_r = \frac{N_m D}{1 - C_m} \frac{\partial C_1}{\partial y} e^{i\omega t}, \tag{6}$$

and combining Eqs. (4) and (6) results in

$$\frac{\partial C_1}{\partial y}\Big|_{y=h} = \frac{i\omega(1 - C_m)}{DN_m} B_s \theta_1. \tag{7}$$

Assuming first-order kinetics, the sorption at the boundary may be expressed as

$$B_s \frac{d\theta}{dt} = k_a c_p (1 - \theta) - k_d \theta, \tag{8}$$

where p is the pressure in the gas mixture, and k_a, k_d denote the adsorption and desorption rate constants, respectively. Since C and p are assumed to be time-harmonic oscillating functions [see Eq. (1)], assuming B_s and $K = k_a/k_d$, where the equilibrium coefficient, K, is a weak function of temperature, we have the following solution for θ:

$$\theta_m = \frac{KC_m p_m}{1 + KC_m p_m}, \tag{9}$$

$$\theta_1 = \frac{K(C_m p_1 + C_1 p_m)(1 - \theta_m)}{1 + KC_m P_m + B_s \hat{\tau}_k^2}, \tag{10}$$

where $\hat{\tau}_k^2 = i\omega/k_a$. The solution for θ_m recovers the classical form of the Langmuir adsorption model [21]. Plugging

Eq. (10) into the boundary condition, Eq. (7), and solving Eq. (2) yields, after some algebra, the solution for the oscillating concentration field,

$$C_1 = -\frac{C_m(1 - H_D)}{p_m \eta_D} p_1 + i \frac{1 - \text{Sc}H_v - \frac{\eta_v}{\eta_D}(1 - H_D)}{A_f \omega F_v (1 - \text{Sc})}$$
$$\times \frac{dC_m}{dx} U_1, \tag{11}$$

where Sc is the *Schmidt* number. Here, the parameter η_n embodies the effect of the sorption kinetics,

$$\eta_n = 1 + h \frac{N_m}{B_s} \frac{(1 - F_n)(1 + KC_m p_m + B_s \hat{\tau}_k^2)(1 + KC_m p_m)}{(1 - C_m)p_m} \tag{12}$$

in which $n = D, v$. We note that $U_1(x)$ is the volumetric flow rate and $A_f = \epsilon A$ is the cross-section area of the gas, in which ϵ is the stack porosity and A is the total cross-section area. The function $H_n(x, y)$ and its cross-section average, $F_n(x)$, has previously been derived for different pore geometries [22] and can be used when solving the thermoacoustic equations, such as ours, with no additional physical assumptions. To match our experimental system, which uses a stack with square channels of size $2h \times 2h$,

these functions are of the following forms:

$$H_n = \frac{1}{\pi^2} \sum_{m,\text{odd}} \frac{\sin^2(m\pi y/2h)}{m^2 J_{n,m}}, \tag{13}$$

$$F_n = \frac{1}{h^2} \int_0^h \int_0^h H_n dx dy = \frac{64}{\pi^4} \sum_{m,\text{odd}} \frac{1}{m^4 J_{n,m}}, \tag{14}$$

$$J_{n,m} = 1 + \frac{\pi^2 m^2}{2\tau_n^2}, \tag{15}$$

where

$$\tau_n \equiv h\sqrt{\omega/n}$$

is a dimensionless parameter representing the ratio of characteristic time scales representing the acoustic oscillations and viscous, conductive and diffusive transport across the channel, represented by $n = \nu, k, D$, respectively. We note that for a different choice of sorption model, η will change its form. The case derived here is an extension of the model used by Weltsch *et al.* [17], recovered in the limit of $\theta \ll 1$ of the current model. Assuming an infinite capacity of the sorbent recovers the case of simple phase change—evaporation and condensation from and to a liquid film, first considered by Raspet *et al.* [23].

B. Heat and mass flux

The nonlinear interaction of oscillating fields can generate nonzero time-averaged quantities, commonly referred to as "steady streaming." In our case, the oscillating velocity field and the oscillating temperature and concentration fields generate a time-averaged heat and mass flux along the sorbing boundary, respectively. This heat flux is the most essential feature for the function of the heat pump described in this work. In general, the streaming flux can be written as $\approx \text{Re}\left[\langle \tilde{U}_1 \xi_1 \rangle\right]$, a time-averaged, second-order transport quantity, in which Re denotes the real part of a complex quantity and the tilde is the complex conjugate. Accordingly, we write the reactive component's mass flux $\dot{m}$ and the total power flux $\dot{H}$ as [24]

$$\dot{m} = \frac{1}{2} M_r N_m \left(\text{Re}\left[\langle \tilde{U}_1 C_1 \rangle\right] - D \frac{dC_m}{dx} \right), \tag{16}$$

and

$$\dot{H} = \frac{1}{2} \rho_m c_p \Re\left[\langle \tilde{U}_1 T_1 \rangle\right] - \left(A_f k_f + A_s k_s\right) \frac{dT_m}{dx} + \dot{m}\ell_h, \tag{17}$$

in which ℓ_h is the adsorption enthalpy of the reactive component, k_f and k_s are the thermal conductivity of the fluid

mixture and solid sorbent, respectively, M_r is the molar density of the reactive component, ρ_m is the mean density of the gas mixture, c_p the constant-pressure heat capacity of the gas mixture, and $As = (1 - \epsilon)A$ is the cross-section area of the solid sorbent. Substituting the solutions for U_1, T_1 [19,24],

$$U_1 = \frac{iA_f F_\nu}{\omega \rho_m} \frac{dp_1}{dx}, \tag{18}$$

$$T_1 = \frac{H_\alpha}{\rho_m c_p} p_1 + \frac{i}{\omega A_f} \frac{dT_m}{dx} \frac{H_\alpha - \text{Pr} H_\nu}{F_\nu(1 - \text{Pr})} U_1, \tag{19}$$

and C_1 into Eqs. (16) and (17) and performing some algebraic manipulations, we derive two ODEs for $C_m(x)$ and $T_m(x)$,

$$\frac{dCm}{dx} = \frac{\frac{1}{2} \frac{C_m}{p_m(1+\text{Sc})} \text{Re}\left[\frac{\tilde{U}_1 p_1}{\eta_D}\left(\frac{F_D - \tilde{F}_\nu}{\tilde{F}_\nu}\right)\right] - \dot{m}\frac{(1-C_m)}{M_r N_m}}{A_f D + \frac{1}{2} \frac{|U_1|^2}{A_f \omega(1-\text{Sc}^2)|F_\nu|^2} \text{Im}\left[\tilde{F}_\nu(1 + \text{Sc}) - \frac{\eta_\nu}{\eta_D}(\tilde{F}_\nu - F_D)\right]}, \tag{20}$$

$$\frac{dT_m}{dx} = \frac{\frac{1}{2}\text{Re}\left[\tilde{U}_1 p_1 \left(\frac{F_\alpha + \text{Pr}\tilde{F}_\nu}{(1+\text{Pr})\tilde{F}_\nu}\right)\right] + \dot{m}\ell_h - \dot{H}}{(A_f k_f + A_s k_s) + \frac{1}{2} \frac{\rho_m c_p |U_1|^2}{A_f \omega(1-\text{Pr}^2)|F_\nu|^2} \text{Im}\left[F_\alpha + \text{Pr}\tilde{F}_\nu\right]}, \tag{21}$$

in which Im denotes the imaginary part of a complex quantity and Pr is the *Prandtl* number.

C. The acoustic field

The final component of the model is the acoustic field—the oscillating pressure and velocity. The acoustic wave equation was previously derived [24], accounting for the presence of a reactive and inert species in the working fluid and a sorbing boundary. Written as separate first-order ODEs for the pressure $p_1(x)$ and the cross-average oscillating volumetric flow rate $U_1(x)$,

$$\frac{dp_1}{dx} = -\frac{i\omega \rho_m}{A_f F_\nu} U_1, \tag{22}$$

$$\frac{dU_1}{dx} = -i\omega \frac{p_1 A_f}{p_m}\left[1 - F_\alpha \frac{\gamma - 1}{\gamma} + \frac{C_m}{1 - C_m}\frac{1 - F_D}{\eta_D}\right]$$
$$- \frac{U_1}{F_\nu}\left[\frac{F_\alpha - F_\nu}{1 - \text{Pr}}\frac{1}{T_m}\frac{dT_m}{dx} + \frac{1 - F_\nu - \frac{\eta_\nu}{\eta_D}(1 - F_D)}{1 - \text{Sc}}\right]$$
$$\times \frac{1}{1 - C_m}\frac{dC_m}{dx}\bigg]. \tag{23}$$

The thermoacoustic Eqs. (21)–(23), describing the acoustic field and the time-averaged temperature distribution in the stack, are derived from the conservation equations for mass, momentum, and energy in the fluid mixture. They are the result of an asymptotic expansion within the framework of the long-wavelength approximation, which is employed to first order in the oscillating quantities. For conciseness, the derivation is left out of this paper, but we refer the interested reader to Ref. [24].

D. Solution methodology

The model consists of four coupled ODEs for the pressure, velocity, temperature, and concentration, namely Eqs. (20)–(23), for p_1, U_1, T_m, C_m as functions of x. Here, we describe the solution methodology applicable to a standing-wave acoustic field driving a heat pump. As such, it involves solving an initial value problem, using a shooting method to enforce physical conditions that match the experimental results. We designate both $\dot{H}$ and $\dot{m}$ as input constants, e.g., $\dot{H}$ is the constant cooling power pumped from the cold side of the stack and removed via a heat exchanger at the "hot" (ambient) side. Similarly, $\dot{m}$ is a constant defined as the rate of mass of the reactive component pumped from the cold side of the stack, and removed in the hot side. The mass flux $\dot{m}$ can be solved for using known boundary values for the concentration of the "reactive" species at both sides of the stack using a shooting method. It is further assumed that the variations of temperature and concentration occur primarily within the stack, and can be neglected in other sections of the resonator.

The system of equations is solved numerically using a fourth-order Runge-Kutta routine implemented in a MATLAB code, along with a shooting method, with the following initial values:

$$p_1(0) = p_A,$$
$$U_1(0) = 0,$$
$$T_m(0) = T_{m,\text{hot}},$$
$$C_m(0) = C_{m,\text{hot}},$$

where p_A is the amplitude of the oscillating pressure.

The concentrations imposed on the system edges are set as the saturation concentration of the reactive component at the cold side and zero concentration in the hot side, i.e., $C_m(0) = 0$ and $C_m(L_s) = C_{m,\text{sat}}$, respectively, and we target the solution for the mass flux that permits these constraints; such boundary conditions constitute "ideal" mass exchanged at the edges. Moreover, to enforce resonant conditions in the quarter-wavelength resonator, we set $p_1(L) = 0$, which is the pressure oscillation at the location of the speaker, and solve for this boundary by shooting on the prescribed frequency by the loudspeaker. The parameter $\hat{\tau}_k^2 = i\omega/k_d$ in Eq. (12) is neglected when

seeking a solution since $k_d \gg \omega$. The solutions are calculated using a value of $\tau_\alpha = \tau_D \cong 3.3$, which is chosen as such as to permit the interaction of most of the volume of gas in each pore with the sorbing plate during each oscillation, which increases the overall efficiency of the system. This value is achieved by changing the pore hydraulic radius h. Moreover, the gas properties at step x are calculated using the temperature at the previous step of the solution $T_m(x - \Delta x)$ so as to decrease the sensitivity of the solutions to the overall mean temperature for all parameters.

IV. RESULTS AND DISCUSSION

A. The mass flux increases the achievable temperature difference

The typical time evolution of the temperature and concentration (of water vapor) can be seen as individual measurements at the hot and cold side (Fig. 4) and as the difference across the stack (Fig. 5). As soon as the acoustic driver is turned on, the temperature difference across the stack develops—the temperature of the cold
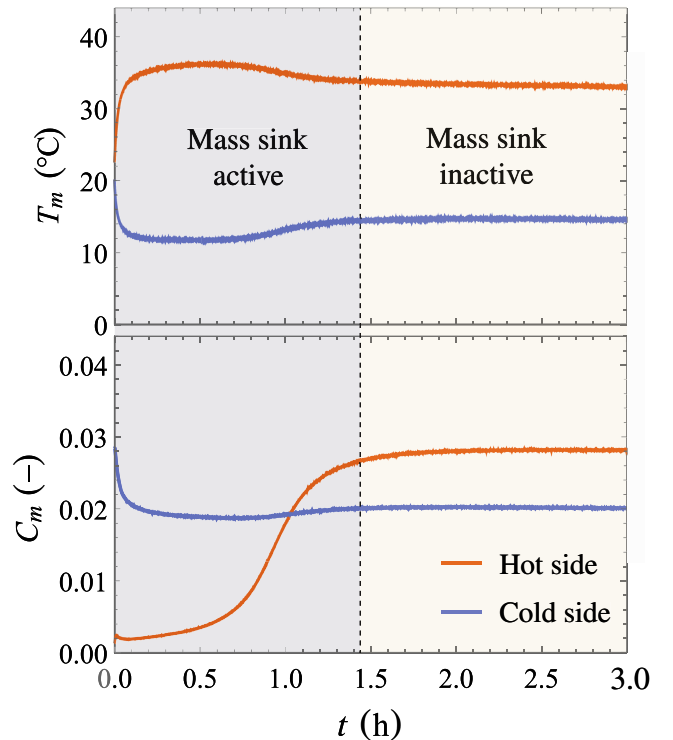

FIG. 4. Representative experimental run, showing the time evolution of the temperatures T_m (in the hot and cold side of the stack) and the molar fraction of the sorbing species C_m (water). The temperature difference is higher when the mole-fraction difference between the hot and cold side is negative, driving a mass flux from the cold to the hot side. This negative concentration difference is maintained as long as the zeolite plug, acting as the mass sink, is active.
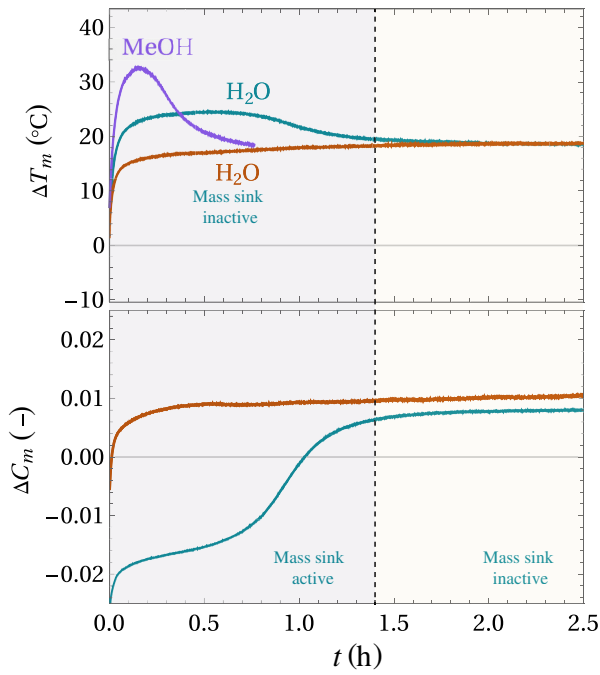
FIG. 5. The temperature difference, ΔT_m, and the concentration difference, ΔC_m as a function of time during operation of the experimental device, as seen in Fig. 4 with an acoustic wave at $f = 122$ Hz, $Q_{\text{cooling}} = 0$ W, and $p_m = 1$ bar, $\dot{E} = 1$ W, in a quarter-wavelength resonator with air as the *inert* gas. Two stages of operation are identified when allowing the use of an active mass sink, where all experiments, with and without an active mass sink, converge to the same temperature differential when the mass sink is inactive.

side decreases, while at the hot side it increases. Considering later times during the experiment, and the measured concentrations, two stages of operation may be identified. During the first stage, vapor is acoustically pumped from the cold side, where saturated conditions are maintained by the liquid pool, to the hot side, where the vapor sink is present. During this stage, mass is transported down the concentration gradient—this is manifested as a negative concentration difference (see bottom panel of Fig. 5). We refer to this stage as one where the mass sink is active. As the experiment progresses, the zeolite sink gradually saturates and the concentration at the hot side increases and eventually surpasses the concentration in the cold side—the gradient is flipped and becomes positive. We mark this as the inactive sink stage, which returns the system back to the classical conduction-based thermoacoustic mechanism [see, again, Figs. 2(c) and 5].

The experiments described are performed without a heat load applied to the system. Therefore, the temperature difference along the stack, ΔT_m, will eventually reach a constant value that reflects its highest possible value, where $\dot{H} = 0$. If the mass flux is generated in the desired direction (from a cold source to a hot sink), we expect an

increase in the temperature difference due to the term $\dot{m}\ell_h$ in Eq. (17), the additional latent heat of adsorption transported along the stack. This is indeed seen during the first stage, which is then followed by a decrease in ΔT_m until a new steady state is reached. This characteristic "hump" in ΔT_m is maintained as long as ΔC_m is negative and relatively constant, and then declines as the concentration difference decreases and then changes sign, at which point the temperatures in the hot and cold side, as well as the corresponding concentrations (which are now the saturation concentrations) reach constant values. This constant ΔT_m is lower since there is no additional mass flux carrying the latent heat—at this stage, $\dot{m} = 0$, the same as the enthalpy flux [17].

This connection between ΔT_m and ΔC_m can be further understood through Eqs. (20) and (21). The lower the concentration gradient, the higher the mass flux along the stack, which accordingly increases the heat flux. To further illustrate this point, experiments are carried out with the zeolite in the plug already saturated with water vapor, making the vapor concentration a function of the temperature alone. This results in a more rapid increase of ΔC_m, which again reaches a limiting value, with a corresponding ΔT_m—identical to the value reached in the second stage of the "regular" experiments.

The experiments are very reproducible, as can be seen in Fig. 6, which shows the measurement range for three experiments performed under three different pressure amplitudes. Furthermore, in these plots the time dependency is removed, instead showing the corresponding values of ΔT_m and ΔC_m at each point in the experiments. Furthermore, in order to test the validity of our derived model, calculations are made based on the actual experimental conditions, with theoretical predictions showing good agreement with the experimental results (see Sec. 3
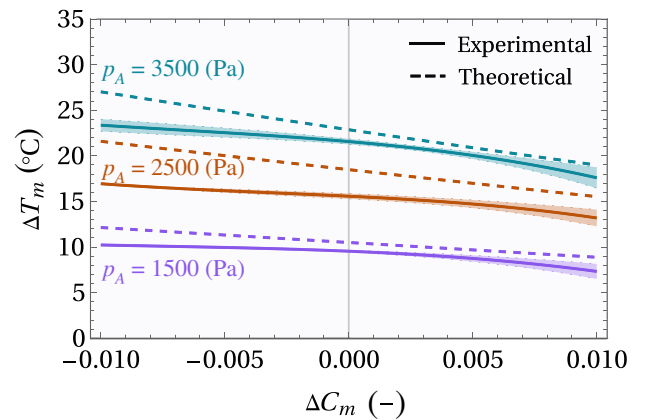

FIG. 6. Mean and standard deviation of experimental measurements made at $f = 122$ Hz and $P_m = 1$ bar, demonstrating the connection between the molar fraction and temperature difference in the stack. Dotted lines show the model calculation.

within the Supplemental Material for more details on these calculations [5]).

B. A higher concentration of the reactive species improves performance

Theory predicts an increased mass flux as C_m, the mean concentration of the sorbing species, is increased [see Eq. (20)]. In order to test this, experiments are performed using methanol (MeOH) as the sorbing species, since it is much more volatile than water. In fact, the water concentration at the cold temperatures reached in our experiments is very low ($C_m \approx 0.02$), which is far from optimal. Indeed, experiments with MeOH show a clear improvement in the ΔT_m achieved, as seen in Fig. 5 (note that these experiments did not include concentration measurements). The temperature "hump" seen for MeOH illustrates the different characteristics of the operation—a sharper, faster increase in ΔT_m; however, the decline is also faster, presumably due to a faster mass flux, which saturates the zeolite plug faster, rendering it inactive quicker. At the same acoustic power, $\Delta T_m = 32.5\,°C$ is measured when MeOH is used, compared with $\Delta T_m = 18\,°C$ when no mass flux is present, illustrating the much better performance of the adsorption-based operation, compared with the "classical," conduction-based thermoacoustic heat pump. A similar, consistent improvement is also observed when using ethanol as the sorbing species (see Fig. S5 within the Supplemental Material [5]). The impact of having a higher molar fraction of the "reactive" species in the mixture may be understood more intuitively by re-examining the schematic representation of the heat-pumping mechanism shown in Fig. 2(b). A higher molar fraction of the sorbing component results in larger oscillations in its partial pressure, inducing a bigger net change in the sorbed and desorbed mass to and from the sorbing boundary, since the concentration is related to the partial pressure via $p_r = CP$, as also manifested by Eq. (10).

C. Measured heat-pump performance

The performance of a heat pump is conventionally quantified through its coefficient of performance (COP), defined as the ratio of the heat flux removed from the system (the heat load, or cooling power) and the power input, which is here taken as the acoustic power input, so that $\text{COP} = \dot{Q}_{\text{cool}}/\dot{E}$. The COP, a measure of efficiency, generally decreases as the temperature difference increases. In order to assess the COP of our system, another set of experiments is conducted, with water-air mixture, in which a heat load is delivered to the cold side of the stack, and the acoustic power delivered to the system is measured (see Fig. S1 within the Supplemental Material for setup visualization [5]). The applied heat load represents the cooling power the heat pump is able to pump against the temperature gradient. In these experiments a given, constant
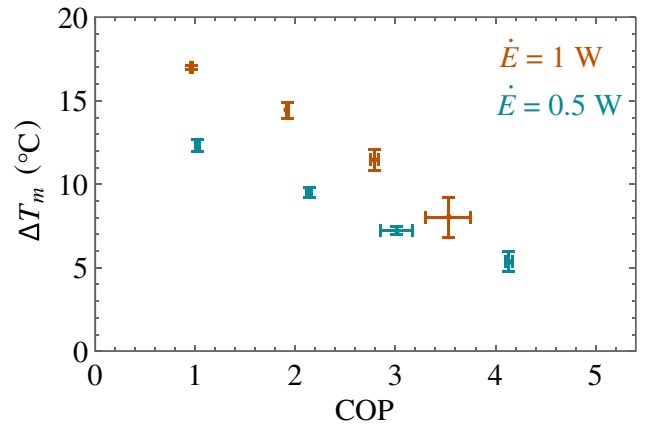

FIG. 7. The temperature difference generated by the system, at a given, imposed coeficcient of performance (COP) of the experimental system, at $f = 122$ Hz and $p_m = 1$ bar with a water-air mixture. The heat load, applied through the nichrome wire, changes the COP measured at each acoustic power, $\dot{E}$, and the maximum temperature difference achieved is measured. Each point represents the mean of the set of experiments, with error bars representing the range of data for each point.

amount of acoustic power is provided, the hot side of the stack remains constant at around $40\,°C$, while the cold-side temperature increases as the cooling power (heating up the cold side) is increased. For each data point, the cooling power is varied at a given acoustic power, and the resulting temperature difference maintained by the system is measured (see Fig. 7). Using 1 W of acoustic power we could achieve a COP of 2, pumping 2 W of heat against a $15\,°C$ temperature difference, which is around 10% of Carnot's efficiency. The COP is equivalently measured for the case when the mass sink is inactive, returning to the classical operation of thermoacoustic cooling. The values for the COPs using this type of operation are much lower for the same temperature difference (see Fig. S9 within the Supplemental Material [5]).

D. Projected coefficient of performance

To better understand the experimental results and, to probe the potential performance of the proposed technology, calculated projections are made using the theoretical model with the geometry and working parameters of the experimental system (which is unoptimized). This is particularly interesting since the current experiments are merely a proof of concept and so the measured performance is likely far below the true potential. In order to probe the potential performance, we opt to perform a sensitivity analysis on one of the τ_n values, which can be τ_α, τ_ν, and τ_D. Careful consideration should be made when optimizing them concurrently, as they are interrelated. For the sake of simplicity, a simple sensitivity analysis of τ_α is made, without consideration for the other two, and was

chosen to be $\tau_\alpha = 3.3$, just as is chosen for our experimental design, keeping all parameters constant. While the system is unoptimized, therefore not fully reflecting its potential, it is worthwhile to note that our theoretical calculations neglect features likely to be present in a fully functioning system, which would reduce performance.

Much like the experiments, the COP is calculated as the ratio between the cooling power $\dot{h} = -\dot{Q}_{\rm cool}$ and the acoustic work input to the system $\dot{E}$ from the acoustic driver. The efficiency of conversion from electric to acoustic power of the driver is not taken into account explicitly in the calculations as we are mainly interested in the COP of the studied mechanism of adsorption-based thermoacoustic refrigeration. We note, however, that the electricacoustic efficiency may be tuned, at a given frequency, to provide high efficiencies, up to and sometimes exceeding 90%, using commercially available linear alternators [26].

Using the full model, numerical calculations are performed for the COP and the relative COP (scaled against the ideal Carnot COP) versus operating ΔT_m (see Fig. 8), examining the effect of different mixtures—the combination of three different sorbate gases—water, methanol, and ethanol) with three inert gases—air, helium, and argon. For the sake of comparison with the state of the art, the figure also shows data gathered by the US Department of Energy (DOE) on the COP of different cooling technologies [25], where the benchmark used was for air-conditioning application using the Air-Conditioning, Heating and Refrigeration Institute standard with a cold-side temperature of 7.2 °C and a hot-side temperature of 40 °C, both being the temperatures of the refrigerant. These data points are used as a reference point with which to frame the results of the introduced technology examined here against the state of the art.

The results show that even without proper optimization, the proposed cooling system can theoretically achieve very high performance using a mixture of methanol and air as the working fluid. We note, however, that the current model does not yet incorporate some elements that may constrain a "real" system and reduce its efficiency. For example, the calculations incorporate the maximum possible concentration gradient imposed on the system, where, in practice, the actual gradient could be lower as it may necessitate a flowing "mass exchanger." Furthermore, heat exchanged with the environment is not optimally addressed, as our system is not insulated.

As already seen in the experimental results, using methanol as the sorbing species achieves the best performance (of the examined materials—other materials may prove to be even better) due to its greater partial pressure at the working temperatures and pressures. For example, using water results in $C_m \sim 0.02$, while for methanol $C_m \sim 0.3$. Furthermore, to retain an appropriate value of τ, when using different inert gases, a higher average pressure is needed at a given channel dimension, $2h$, which in turn

decreases the overall average molar fraction of the sorbing component. Therefore, when using heavier gases, which in our case is air, a lower operating pressure is needed and a higher average molar fraction is achieved along with better theoretical COP. Although a higher average C_m in the resonator can result in much improved performance, the use of a high-pressure working gas can allow the reduction in pore size and the increase of surface area available to work with (again, by keeping τ optimized) making the overall reduction of the physical form factor possible. Therefore, careful consideration of the working gas mixture is needed, to allow a high average C_m along with a high mean pressure p_m, to find the best performance possible in small form factors.

We continue by considering the upper limit of the theoretical COP, using a simplified derivation based on our model. This is done to better understand how the COP is affected by the introduced mechanism. The total power absorbed along the length of the stack, L_s, may be written as [9]

$$\Delta \dot{E} = \frac{L_s}{2} {\rm Re} \left[p_1 \frac{d\tilde{u}_1}{dx} + \frac{dp_1}{dx} \tilde{u}_1 \right].\qquad(24)$$

The maximum efficiency is considered here at low-temperature gradients, and it decreases monotonically with increasing temperature gradients. For the sake of simplicity, we assume pure standing-wave phasing between the velocity and pressure, such that $U_1 \sim -iP_1$. Furthermore, viscous losses are neglected, so that $F_\nu \to 1$. Taking the limit of $\tau_n \gg 1$ (the "boundary-layer" limit [9]), and applying these assumptions to Eq. (24), using Eqs. (22) and (23), as well as to the expression for $\dot{H}$, results in the following, approximate form for the COP (see Sec. 7 within the Supplemental Material for the full derivation [5]):

$$\text{COP} = \frac{\dot{H}}{\Delta \dot{E}} \sim \frac{|U_1| p_m}{\omega L_s |p_1|} \left[\frac{1 + \frac{\ell_h}{{\rm R} T_m} \frac{C_m}{1 - C_m}}{1 + \frac{C_m}{(1 - C_m)}} \right],\qquad(25)$$

which shows that the efficiency of the system, at low-temperature gradients, increases with the mean pressure but decreases with frequency. It also shows that a major factor, as expected, is the latent heat and molar fraction of the sorbing component. The acoustic field is manifested through the pressure and velocity amplitudes. The choice of T_m can be arbitrary along the stack, as the values for the COP calculated using Eq. (25) is not heavily affected by it. We choose T_m to be the temperature on the cold side of the stack. While the ratio of acoustic velocity and pressure should be maximized in this idealized scenario, in practice the increase in velocity results in larger viscous dissipation, and so a compromise is necessary.

While the existence of a sorption-based cooling mechanism has been clearly demonstrated, further development
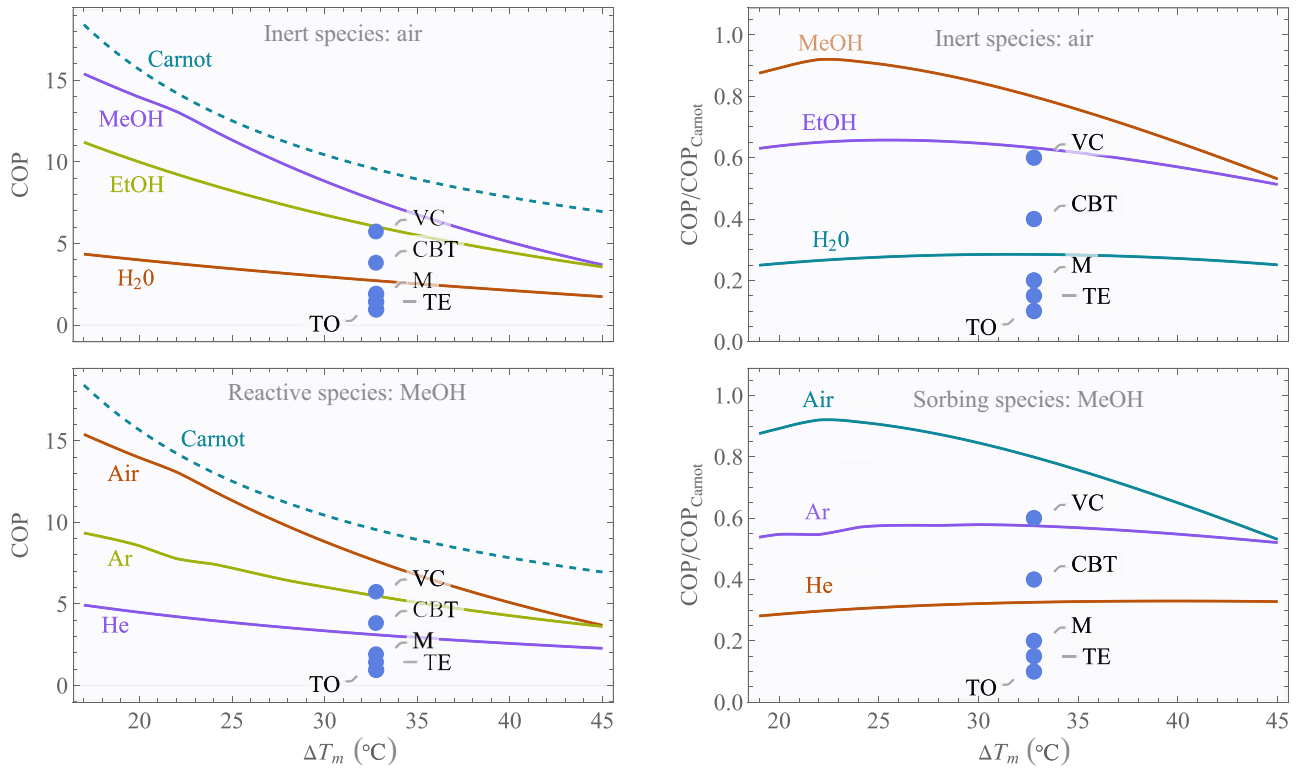
FIG. 8. Theoretical calculations of (a) the COP versus temperature difference. (b) The relative COP (ratio of the COP to the Carnot limit) versus the temperature difference. Calculations are based on the properties of the experimental heat-pump system described in Fig. 2(a) calculated with a nominal heat load of $Q_{cool} = 5$ W and $T_{m,hot} = 40\,°C$, with $\tau_\alpha \cong 3.3$. The calculations examine different gas mixtures comprised of various combinations of "inert" (air, helium, and argon) and "sorbing" (water, methanol, and ethanol) species. The Carnot COP is also plotted versus the temperature difference. The computed COP is compared with the highest practical and theoretical COP achievable by different cooling technologies in existence today [25], labeled as follows: TO, thermionic; TE, thermoelectric; M, magnetocaloric; CBT, conduction-based thermoacoustics; VC, vapor compression.

is needed to allow its continuous operation. For example, the implementation of a mass exchanger, able to deliver mass of a sorbing component at the cold side, and removing mass at the hot side. In the mathematical model, we assume a Langmuir-type sorption model, which is not necessarily the best choice for the operation of the cooling cycle. Furthermore, the model requires some refinement to properly capture an absorption system, although for parameter ranges beneficial to the cooling cycle, the current model should suffice. Finally, operation in a traveling acoustic wave field should also be considered, as previous studies demonstrated its the ability to increase the mass flux [18].

V. SUMMARY AND CONCLUSIONS

Motivated by the growing need for sustainable, environmentally benign small-scale cooling technology, we examine the potential of a sorption-based, acoustically driven heat pump. Such a system encompasses the advantages of thermoacoustics—simple, reliable construction with little to no moving parts, with the increased efficiency and

environmentally benign materials offered by sorption. An experimental apparatus is constructed and serves as an initial proof of concept of the mechanism involved, which is confirmed by a mathematical model of the heat and mass transfer within the acoustic field. The model is then used to probe the main parameters involved and consider the projected performance of this technology.

Experimental results demonstrated the heat-pumping mechanism involving a time-averaged mass flux resulting from the reversible sorption process by which mass is exchanged between the gas mixture and the solid. The heat flux generates temperature differentials, which are shown to increase as a function of the molar fraction of the sorbing species in the gas mixture used. Our unoptimized system is capable of generating appreciable temperature differentials at very encouraging efficiencies, for example, maintaining $\Delta T \sim 10$ with a COP ~ 3, using humid air as the working fluid. These results encourage further investigations into potential improvement avenues, including the effects of sorption kinetics, alternative gas mixtures, operating parameters such as geometrical properties, mean pressure, and stack composition, as well as the acoustic field itself.

While the current work demonstrates the use of an adsorption-based stack and batch mass exchanger, we note that this process is equally realizable using absorption. More encompassing work was done recently, demonstrating great improvements in performance of thermoacoustic heat pumps employing phase change [27]. Moving from the batch mode, used here as a proof of concept, to continuous operation would necessitate use of mass exchangers introducing and removing material at the ends of the stack. Such a setup may be more easily realizable using liquid absorbents, for example, via membrane-based contactors in which the sorbing fluid is circulated (e.g., H_2O-LiBr, NH_4-$LiNO_3$) [28,29]. This can allow the continuous operation of the system by pumping the absorbing liquid through the membrane, removing the reactive mass and heat from the hot side of the stack. Such operation can be achieved by a counter-current mode, where two streams are used such that they cogenerate each other over a few stages (though the overall average concentration gradient along the stack is reduced). We note that the transition from a batch-mode operation, as demonstrated in this paper, to a continuous operation using any of the proposed solutions we propose in this section will inherently reduce the COP achievable in the system. This is true when incorporating any mass or heat exchanger in a complete and fully functional refrigerator. As another example, soaking the stack with an absorbing liquid can also be used to allow the stack to function in an absorption process instead of adsorption. These few examples show the potential for further research directions surrounding acoustic driven sorption cooling, which go beyond the scope of the present work. At this point, it is unclear what the impact of the regeneration would be exactly, and we focus our attention to the potential of the system, while making it clear that it represents an upper bound.

Model calculations demonstrate the remarkably high potential presented by this sorption-based mechanism, with the COP reaching 70% of the Carnot limit. Optimization of the process, acoustic phasing, and working fluid may further improve efficiency, however, parasitic viscous and heat losses, for example, due to the mass exchangers, as well as the regeneration of sorbents (which is possible in a multistage configuration) will offset the efficiency. Considering other attributes of thermoacoustic technology, its relatively simple construction with little to no moving parts, its use of simple, environmentally benign materials, and ability to operate with either heat or electric energy input offers exciting prospects for further development of this sorption-based acoustic device.

ACKNOWLEDGMENTS

[1] IEA, *The Future of Cooling* (IEA, 2018).

[2] R. Khosla, N. D. Miranda, P. A. Trotter, A. Mazzone, R. Renaldi, C. McElroy, F. Cohen, A. Jani, R. Perera-Salazar, and M. McCulloch, Cooling for sustainable development, Nat. Sustainability **4**, 201 (2021).

[3] M. Protocol, Montreal protocol on substances that deplete the ozone layer, Washington, DC: US Government Printing Office **26**, 128 (1987).

[4] P. Hawken, *Drawdown: The Most Comprehensive Plan Ever Proposed to Reverse Global Warming* (Penguin, London, 2017).

[5] See Supplemental Material at http://link.aps.org/supplemental/10.1103/PhysRevApplied.16.044044 for more detailed information on mathematical derivations, experimental setup, and more (2021).

[6] M. Wetzel and C. Herman, Design optimization of thermoacoustic refrigerators, Int. J. Refrigeration **20**, 3 (1997).

[7] Y. Huang, E. Luo, W. Dai, and Z. Wu, in *Cryocoolers 13*, edited by R. G. Ross (Springer US, Boston, MA, 2005), p. 189.

[8] S. L. Garrett, J. A. Adeff, and T. J. Hofler, Thermoacoustic refrigerator for space applications, J. Thermophys. Heat Transfer **7**, 595 (1993).

[9] G. W. Swift, Thermoacoustic engines, J. Acoust. Soc. Am. **84**, 1145 (1988).

[10] A. Meir, A. Offner, and G. Z. Ramon, Low-temperature energy conversion using a phase-change acoustic heat engine, Appl. Energy **231**, 372 (2018).

[11] R. Yang, A. Meir, and G. Z. Ramon, Theoretical performance characteristics of a travelling-wave phase-change thermoacoustic engine for low-grade heat recovery, Appl. Energy **261**, 114377 (2020).

[12] Nasa - double-fed induction linear alternator (U.S. Patent 10, 581, 355, 2016).

[13] H. Tijani, J. Zeegers, and A. De Waele, Design of thermoacoustic refrigerators, Cryogenics **42**, 49 (2002).

[14] A. Allouhi, T. Kousksou, A. Jamil, P. Bruel, Y. Mourad, and Y. Zeraouli, Solar driven cooling systems: An updated review, Renewable and Sustainable Energy Rev. **44**, 159 (2015).

[15] H. Demir, M. Mobedi, and S. Ülkü, A review on adsorption heat pump: Problems and solutions, Renewable and Sustainable Energy Rev. **12**, 2381 (2008).

[16] N. A. Zolpakar, N. Mohd-Ghazali, and M. Hassan El-Fawal, Performance analysis of the standing wave thermoacoustic refrigerator: A review, Renewable and Sustainable Energy Rev. **54**, 626 (2016).

[17] O. Weltsch, A. Offner, D. Liberzon, and G. Z. Ramon, Adsorption-Mediated Mass Streaming in a Standing Acoustic Wave, Phys. Rev. Lett. **118**, 1 (2017).

[18] Y. Blayer, N. Elkayam, and G. Z. Ramon, Phase-dependence of sorption-induced mass streaming in an acoustic field, Appl. Phys. Lett. **115**, 033703 (2019).

[19] G. W. Swift, Thermoacoustics: A unifying perspective for some engines and refrigerators (Springer, New York, 2002).

[20] A. M. Fusco, W. C. Ward, and G. W. Swift, Two-sensor power measurements in lossy ducts, J. Acoust. Soc. Am. **91**, 2229 (1992).

[21] H.-J. Butt, K. Graf, and M. Kappl, *Physics and Chemistry of Interfaces* (John Wiley & Sons, London, 2013).

[22] W. P. Arnott, H. E. Bass, and R. Raspet, General formulation of thermoacoustics for stacks having arbitrarily shaped pore cross sections, J. Acoust. Soc. Am. **90**, 3228 (1991).

[23] R. Raspet, W. V. Slaton, C. J. Hickey, and R. A. Hiller, Theory of inert gas-condensing vapor thermoacoustics: Propagation equation, J. Acoust. Soc. Am. **112**, 1414 (2002).

[24] A. Offner, R. Yang, D. Felman, N. Elkayam, Y. Agnon, and G. Z. Ramon, Acoustic oscillations driven by boundary mass exchange, J. Fluid. Mech. **866**, 316 (2019).

[25] D. R. Brown, T. Stout, J. A. Dirks, and N. Fernandez, The prospects of alternatives to vapor compression technology for space cooling and food refrigeration applications, Energy Eng. **109**, 7 (2012).

[26] J. A. Corey and G. A. Yarr, *HOTS to WATTS: The FPSE linear alternator system re-invented*, type Tech. Rep. (institution SAE Technical Paper, 1992).

[27] R. Yang, N. Blanc, and G. Z. Ramon, Environmentally-sound: An acoustic-driven heat pump based on phase change, Energy Convers. Manage. **232**, 113848 (2021).

[28] N. García-Hernando, M. De Vega, and M. Venegas, Experimental characterisation of a novel adiabatic membrane-based micro-absorber using h2o-libr, Int. J. Heat. Mass. Transf. **129**, 1136 (2019).

[29] F. Asfand and M. Bourouis, A review of membrane contactors applied in absorption refrigeration systems, Renewable and Sustainable Energy Rev. **45**, 173 (2015).